Available online at www.sciencedirect.com
SCIENCE DIRECT®
International Journal of Pharmaceutics 269 (2004) 211–225
international journal of pharmaceutics
www.elsevier.com/locate/ijpharm

The influence of transferrin stabilised magnetic nanoparticles on human dermal fibroblasts in culture

Catherine C. Berry [a,*], Stuart Charles [b], Stephen Wells [b], Matthew J. Dalby [a], Adam S.G. Curtis [a]

[a] *Centre for Cell Engineering, Institute of Biomedical and Life Sciences, University of Glasgow, Joseph Black Building, Glasgow G12 8QQ, UK*
[b] *Liquids Research Limited, Unit 3B, Mentec, Deiniol Road, Bangor, Gwynedd, North Wales LL57 2UP, UK*

Received 29 April 2003; received in revised form 2 August 2003; accepted 5 September 2003

Abstract

Magnetic nanoparticles have been used for bio-medical purposes including drug delivery, cell destruction and as MRI contrast agents for several years. A more recent biological application has focused on targeted drug delivery. To this end, a wide variety of iron oxide nanoparticles have been synthesised. This study involves the use of magnetic nanoparticles synthesised and derivatised with human transferrin, compared to identical underivatised particles. Human fibroblasts were used, representative of a tissue cell-type. The influence in vitro was determined using light and fluorescence microscopy, scanning and transmission electron microscopy, and 1718 gene microarray. The results indicate that the transferrin derivatised particles appear to localise to the cell membrane without instigating receptor-mediated endocytosis, and also induce up-regulation in the cells for many genes, particularly in the area of cytoskeleton and cell signalling. The microscopy results further support these findings.

Keywords: Magnetic nanoparticles; Drug delivery; Transferrin; Cell response; Microarray

1. Introduction

The application of small particles in in vitro diagnostics has been practised for nearly 40 years due to a number of beneficial factors including a large surface area to volume ratio, and the possibility of ubiquitous tissue accessibility (Lacava et al., 2001; Babes et al., 1999). In the last decade increased investigations and developments were observed in the field of nanosized magnetic particles (≤1 μm in size, and normally below 500 nm). In recent years, nanotechnology has developed to a stage that makes it possible to produce, characterise and specifically tailor the functional properties of nanoparticles for clinical applications, such as targeted drug delivery systems (Curtis and Wilkinson, 2001; Moghimi et al., 2001).

The main problems currently associated with systemic drug administration include even biodistribution of pharmaceuticals throughout the body, lack of drug specificity towards a pathological site, the necessity of a large dose to achieve high local concentration, non-specific toxicity and other adverse side effects due to high drug doses. Drug targeting aims to resolve many of these problems (Torchilin, 2000). The use of magnetic systems could potentially overcome the hurdle of attracting and targeting particles to a particular

* Corresponding author. Tel.: +44-141-330-3550; fax: +44-141-330-3730.
E-mail address: catherine.berry@bio.gla.ac.uk (C.C. Berry).

0378-5173/$ – see front matter © 2003 Elsevier B.V. All rights reserved.
doi:10.1016/j.ijpharm.2003.09.042

site in the body whilst maintaining local levels until the therapy is complete. In particular, superparamagnetic particles are of interest, as they do not retain any magnetism after removal of a magnetic field, and larger domain magnetic/paramagnetic materials tend to aggregate after exposure to a magnetic field (Wang et al., 2001; Bonnemain, 1998).

Studies on different iron oxide MRI contrast agents have shown that the biodistribution depends on the coating of the particle (Chouly et al., 1996). A further problem encountered is the threat of endocytosis/phagocytosis from reticuloendothelial system (RES) macrophages, which occurs after particles are injected into the bloodstream and are rapidly coated by components of the circulation, such as plasma proteins (Morrissette et al., 1999). This process, known as opsonisation, is critical in dictating the circumstance of the injected particles (Davis, 1997). This rapid sequestration of particles has prompted the search for 'macrophage-evading' or long-circulating particles (Moghimi et al., 2001).

To this end, a wide variety of iron oxide nanoparticles have been synthesised. They differ in type of coating material used, including dextran, starch, albumin, and silicones, and also in size, resulting in hydrodynamic particle size varying between 10 and 3500 nm (Babes et al., 1999) to varying success. A highly publicised example of magnetic drug delivery is as a replacement or to augment chemotherapy/radiotherapy treatments. The first clinical trials in humans with a magnetic drug targeting worldwide were reported by Lubbe et al. (1999), who used a ferrofluid (particle size 100 nm) to which the drug epirubicin was chemically bound to treat solid tumours. It was shown that the ferrofluid could be successfully directed to the tumours in about half of the patients. The in vivo performance of the nanoparticles could, however, be improved further by modification of the coating (Lubbe et al., 2001). For example, as the adhesiveness of the particles is considered to be a major factor increasing the bioavailability and reducing variability in absorption, targeting to cell membrane receptors may prove advantageous (Muller et al., 2001).

In this study, iron oxide nanoparticles (8–15 nm) were synthesised and derivatised with human transferrin. Since transferrin was discovered more than half a century ago, a considerable effort has been made towards understanding transferrin-mediated iron uptake (Fulimoto et al., 2000). Apart from iron, many other metal ions of therapeutic and diagnositc interest can also bind to transferrin at the iron sites and their resultant transferrin complexes can be recognised by many cells (Li and Qian, 2002). Therefore, transferrin has been thought of as a 'delivery system' into cells. In addition, it has also been widely applied as a targeting ligand in the active targeting of anticancer agents, proteins and genes to primary proliferating cells via transferrin receptors (Moore et al., 2001; Bulte et al., 1999).

This paper investigated the influence of the synthesised transferrin derivatised nanoparticles on human dermal fibroblasts in vitro, as compared to underivatised. This was achieved in terms of cell morphology, cell proliferation and scanning and transmission electron microscopy (SEM/TEM) studies. The possibility of particle uptake via endocytosis was investigated utilising fluorescent microscopy to observe both the cell cytoskeleton (F-actin and tubulin) and clathrin localisation, and also the quantification of fluorescently labelled particle uptake and CD71 (transferrin receptor) on the cell surface. Finally human 1718 cDNA microarrays were also used to measure the gene response to the nanoparticles. The findings showed that the underivatised particles were rapidly endocytosed into the cell causing disruption to the cell cytoskeleton and a decrease in proliferation. The transferrin derivatised nanoparticles, however, stimulated cell proliferation, and were not internalised as would be expected, but appeared to attach to the outside of the cell membrane, most likely to cell expressed transferrin receptors.

2. Materials and methods

2.1. Nanoparticle production

Magnetite nanoparticles of approximately 10 nm diameter were precipitated in alkali solution from solutions of Fe(II) and Fe(III) chloride according to the standard co-precipitation technique of Khalafalla and Reimers (Reimers and Khalafalla, 1972). The magnetic nanoparticles can be colloidally stabilised by the addition of oleic acid (a long chain surfactant) according to reference 18.

The prepared nanoparticles were washed with deionised water and coated with transferrin (Sigma, UK) by Liquids Research Ltd. at a transferrin magnetite w/w ratio of 3:1, with coupling believed to be by the organic group, and were then dispersed in water. Magnetic particle size measurements have been routinely undertaken using a vibrating sample magnetometer (VSM—results not shown here). The physical particle size was determined via transmission electron microscopy (TEM, Zeiss 902, voltage −80 kV), where an aqueous dispersion of the particles was drop cast onto a carbon coated copper grid, which was subsequently air dried at room temperature before loading into the microscope.

2.2. Cell culture

Infinity™ Telomerase Immortalised primary human fibroblasts (hTERT-BJ1, Clonetech Laboratories, Inc., USA) were seeded onto glass coverslips (13 mm diameter) at a density of 1×10^4 cells per disk in 1 ml of complete medium. The medium used was 71% Dulbeccos Modified Eagles Medium (DMEM) (Sigma), 17.5% Medium 199 (Sigma), 9% foetal calf serum (FCS) (Life Technologies, UK), 1.6% 200 mM L-glutamine (Life Technologies, UK) and 0.9% 100 mM sodium pyruvate (Life Technologies, UK). The cells were incubated at 37 °C with a 5% CO_2 atmosphere for 24 h. At this time point the cells were incubated in complete medium supplemented with 0.05 mg ml^{-1} transferrin derivatised (TfD) and underivatised plain (P) nanoparticles for a further specified time. All control cells were cultured in the absence of any particles.

2.3. Light microscopy staining for cell morphology

The fibroblasts were cultured in the presence of both particles for up to 24 h. At each time point, the cells were washed in phosphate buffered saline (PBS) and then fixed in 4% formaldehyde/PBS for 15 min at 37 °C. The cells were subsequently stained for 2 min in 0.5% Coomassie blue in a methanol/acetic acid aqueous solution, and washed with double distilled water to remove excess dye. Samples could then be observed by light microscopy, and digital images were captured using a Hamamatsu Argus 20 for image processing. Control cells were cultured in complete medium only.

2.4. Bromodeoxyuridine (BrdU) incorporation for cell proliferation

The fibroblasts were cultured in the presence of both types of nanoparticles for up to 72 h with complete medium further supplemented with bromodeoxyuridine. At 24, 48 and 72 h time points, the cells were PBS washed and fixed in 4% formaldehyde/PBS for 15 min at 37 °C. Cells were then washed with PBS, and a permeabilising buffer (10.3 g sucrose, 0.292 g NaCl, 0.06 g $MgCl_2$, 0.476 g Hepes buffer, 0.5 ml Triton-X, in 100 ml water, pH 7.2) added at 4 °C for 5 min. The samples were then incubated at 37 °C for 5 min in 1% BSA/PBS. This was followed by the addition of anti-BrdU primary antibody (1:100 in 1% BSA/PBS, monoclonal anti-human raised in mouse (IgG1), Sigma) for 1 h (37 °C). The samples were next washed in 0.5% Tween 20/PBS (5 min × 3). A secondary, biotin conjugated antibody (1:50 in 1% BSA/PBS, monoclonal horse anti-mouse (IgG), Vector Laboratories, UK) was added for 1 h (37 °C) followed by washing. A FITC conjugated streptavidin third layer was added (1:50 in 1% BSA/PBS, Vector Laboratories, UK) at 4 °C for 30 min, and given a final wash. Samples were then viewed by fluorescence microscope (Vickers M17). Proliferating cells were determined by stained nuclei, and were counted per microscopic field and expressed as a percentage as compared to control cells cultured only in complete medium.

2.5. Scanning electron microscopy (SEM)

The cells were fixed with 1.5% gluteraldehyde (Sigma) buffered in 0.1 M sodium cacodylate (Agar, UK) (4 °C, 1 h) after a 24 and 48 h incubation in both particles. The cells were then post-fixed in 1% osmium tetroxide for 1 h (Agar, UK) and 1% tannic acid (Agar, UK) was used as a mordanant. Samples were dehydrated through a series of alcohol concentrations (20, 30, 40, 50, 60, 70%), stained in 0.5% uranyl acetate, followed by further dehydration (90, 96, 100% alcohol). The final dehydration was in hexamethyl-disilazane (Sigma), followed by air-drying. Once dry, the samples were sputter coated with gold before examination with a Hitachi S800 field emission SEM at an accelerating voltage of 10 keV.

2.6. Transmission electron microscopy (TEM)

The cells were cultured in three dimensional type I collagen gel culture, a common 3D model system (Bell et al., 1979). A 10 nml aliquot of cell seeded collagen gel was prepared by the addition of 4 ml DMEM (2×) (Life technologies, UK), 3 ml collagen solution (3 mg ml^{-1} in acetic acid. Cellagen AC-1, ICN Biomedicals, UK), 1 ml of 10% FCS, 1 ml of 0.1 M sodium hydroxide (Sigma) and 1 ml of cell suspension. All solutions were kept on ice prior to mixing. Cell seeded gels were cast as 0.5 ml aliquots into a 24-well plate, with a final concentration of 3×10^5 cells per ml of gel. Three sets of gels were cast, a control set, and two sets with 0.05 mg ml^{-1} P or TfD nanoparticles infused through the mixture. The gels were set at 37 °C for 30 min, detached from the edge of the well (to allow multiaxial gel contraction) (Grinnell and Lamke, 1984; Nakagawa et al., 1989) and cultured for a further 5 days incubated at 37 °C with a 5% CO_2 atmosphere.

Collagen gels were fixed as for SEM, and cut into smaller sections for processing. The gels were then stained for 60 min with 1% osmium tetroxide and then taken directly through the alcohol steps up to dried absolute alcohol as for SEM. The gels were then treated with 1:1 dried absolute alcohol:resin overnight to evaporate the alcohol. The gels were subsequently embedded in Spur's resin, and ultra-thin sections were cut and stained with lead nitrate and viewed under a Zeiss 902 electron microscope at 80 kV.

2.7. Evidence of particle uptake

2.7.1. Clathrin immunofluorescence and cytoskeletal observation: 37 and 4 °C

Cells were cultured with both types of nanoparticle for 30 min at either 37 or 4 °C. Cells were subsequently fixed in 4% formaldehyde/PBS, with 1% sucrose at 37 °C for 15 min. The samples were then washed with PBS, and permeabilising buffer was added at 4 °C for 5 min. The samples were then incubated at 37 °C for 5 min in 1% BSA/PBS. This was followed by the addition of anti-tubulin or anti-clathrin primary antibody (1:100 in 1% BSA/PBS, monoclonal anti-human raised in mouse (IgG1), Sigma) for 1 h (37 °C). Simultaneously, rhodamine conjugated phalloidin was added for the duration of this incubation (1:100 in 1% BSA/PBS, Molecular Probes, Oregon, USA). The samples were then washed in 0.5% Tween 20/PBS and a secondary, biotin conjugated antibody (1:50 in 1% BSA/PBS, monoclonal horse anti-mouse (IgG), Vector Laboratories, UK) was added for 1 h (37 °C) followed by more washing. A FITC conjugated streptavidin third layer was added (1:50 in 1% BSA/PBS, Vector Laboratories, UK) at 4 °C for 30 min, and given a final wash. Samples were then viewed by fluorescence microscope (Vickers M17) with images captured using a Hamamatsu Argus 20.

2.7.2. Quantification of fluorescently labelled particle uptake

Particle uptake was verified by fluorescently coating the nanoparticles followed by observation using fluorescence microscopy. The method was adapted form a technical immunology book (Michell and Shiigi, 1980). Briefly, both P and TfD nanoparticles were dialysed against 0.15 M sodium chloride (three changes of solution over 2 days), followed by dialysis against 0.05 M bicarbonate buffered saline (BBS, pH 8.5) for 5 h and a final dialysis against 0.05 M BBS (pH 9.2) for 2 h. The particles were then dialysed against 100 μg of the fluorochrome fluorescein-5-isothiocyanate (FITC, Molecular Probes) in 0.05 M BBS (pH 9.2) for a further 14–16 h (with the volume of the 'chrome' exactly 10 times that of the sample). Finally, the above reaction was halted by dialysis against 0.02 M phosphate buffered saline (PBS, pH 7.0) for 2–3 h. Note that all dialysis was performed at 4 °C.

Cells were subsequently incubated in the particles for 30 min and samples viewed by fluorescence microscope (Vickers M17) with images captured using a Hamamatsu Argus 20. For quantification of particle uptake an in-house method was then used that relied on ImageJ imaging software downloaded from the National Institute of Health (USA) (NIH Image-free download available at http://www.rsb.info.nih.gov/nih-image). This used automated detection of the intensity of stain per image, with five cells counted for four replicates (note that standardised illumination conditions were used throughout). Student's *t*-test (for two samples assuming unequal variance) was used to compare statistical significance of the control cells with those incubated in P and TfD nanoparticles (differences: $^*P \leq 0.05$).

2.8. RNA expression analysis

Individual gene expression changes were detected by using spotted DNA microarrays. The arrays were printed with 1718 distinct human transcripts obtained from the Ontario Cancer Institute Microarray Centre (http://www.uhnres.utoronto.ca/services/microarray/products.html). Complete protocols for the generation of fluorescence labelled samples from whole cell RNA, hybridisation to DNA microarrays and data processing can be found at this web site.

Briefly, cells were cultured with/without the P and TfD nanoparticles for 48 h on six-well culture plates, to allow extraction of sufficient amounts of RNA (four wells per treatment). At this point cells were lysed and total RNA was extracted using a Qiagen RNeasy kit (Qiagen, UK) according to manufacturers instructions. The RNA was used to make CY 3- or CY 5-labelled cDNA (Amersham Pharmacia, UK) using Superscript II reverse transcriptase with a poly-T mRNA primer (Gibco BRL, UK). For two of the arrays, the controls were labelled with CY 5 and the test samples with CY 3, for the third array, the controls were labelled with CY 3 and the test samples with CY 5. This 'fluor-flip' ensures that the results are not artefacts of which dyes were used for the controls and samples (i.e. the results must be the same with each 'flip' in order to be accepted). Samples were prepared for hybridisation by combining fragmented salmon sperm DNA ($0.5\,\mu g\,\mu l^{-1}$; Gibco BRL, UK) and yeast tRNA ($0.5\,\mu g\,\mu l^{-1}$; Gibco BRL, UK) in EasyHyb solution (Roche Diagnostics, UK). Samples were hybridised for 16 h at 37 °C onto four cDNA microarrays containing 1718 known human expressed sequence tags. Arrays were next washed three times at room temperature with 0.1% (v/v) saline sodium citrate (SSC) containing 0.1% (v/v) SDS followed by one wash with 0.1% SSC alone.

Fluorescence intensities were captured using Packard Scanarray Lite laser confocal scanner. Expression data were analysed as described by Eisen et al. (1998). For each gene, the arrays were spotted in duplicate, and only where both spots on all three slides were in agreement was the result accepted, and then only if the change was greater than 50% from the control data. Gene changes conforming to these restrictions for the following headings are reported: cytoskeleton, extracellular matrix, DNA replication and cell signalling.

2.9. Quantification of CD71 levels

Following 6 h culture, the cells were fixed, permeabolised and blocked with 1% BSA/PBS as Section 2.6. Cells were then incubated with the primary antibody anti-CD71 for 1 h at 37 °C ($0.1\,mg\,ml^{-1}$ used neat, ab7530, abcam, UK). Subsequent incubations with a secondary and tertiary were as Section 2.6. Samples could then be observed by fluorescence microscopy, and digital images were captured using a Hamamatsu Argus 20 for image processing. Levels of CD71 were quantified using ImageJ (as in Section 2.7.2). This used automated detection of the intensity of stain per image, with five cells counted for four replicates (note that standardised illumination conditions were used throughout). Student's *t*-test (for two samples assuming unequal variance) was used to compare statistical

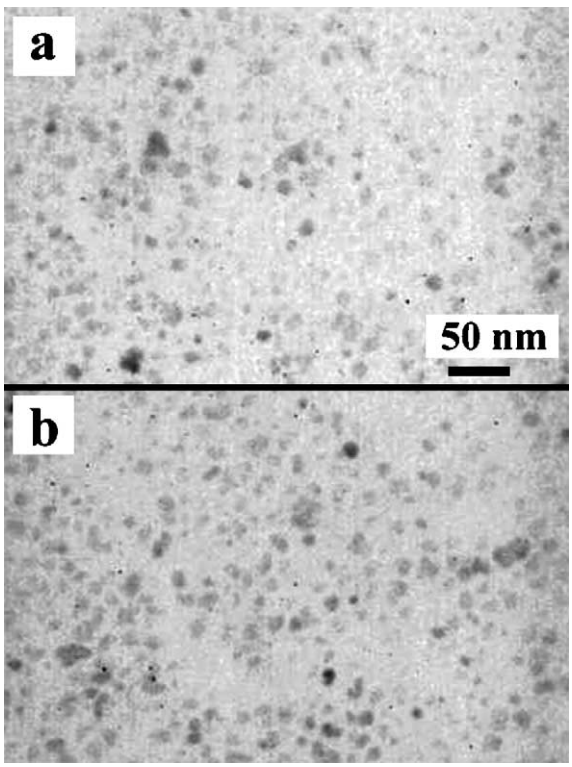

Fig. 1. TEM image of (a) P particles and (b) TfD particles.

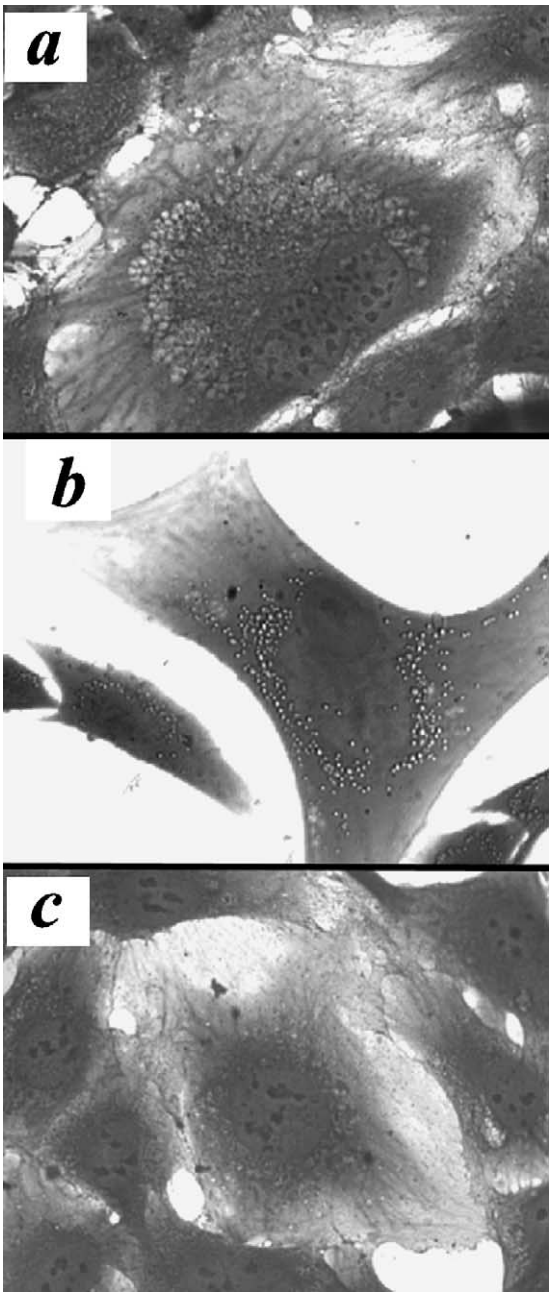

Fig. 2. Coomassie staining of (a) control cells, (b) cells incubated with P nanoparticles and (c) cells incubated with TfD nanoparticles after 24 h culture.

significance of the cells incubated in the transferrin derivatised particles with control cells (differences: * $P \leq 0.05$).

3. Results

The nanoparticle production method results in a fluid that is dilution stable, which can only occur if the transferrin has coated the particles so that sufficient entropic repulsion is provided to overcome van der waals forces and magnetic interactions. TEM images of the magnetic nanoparticles was used to determine the shape, size and uniformity of the particles (Fig. 1). The figure shows that the particles are spherical shaped and monodispersed with an approximate size distribution between 10 and 15 nm.

Incubation with the P particles clearly caused the appearance of vacuoles in the cell body, as shown with the Coomassie blue staining, whereas the TfD particles had no effect on gross cell morphology (Fig. 2). The BrdU incorporation results, reflecting cell proliferation, indicated that an increase in cell proliferation was evident with increasing time in culture with the TfD nanoparticles as opposed to a decrease observed with the P nanoparticles, compared to control cells (Fig. 3).

SEM observation of cell morphology for control cells demonstrated flattened, spread cells with lamellapodia at both 24 and 48 h (Fig. 4a and d). The cells exposed to P nanoparticles, however, exhibited aberrations on the cell membrane, possibly indicative of particle internalisation, with a highly disrupted cell morphology after 48 h incubation (Fig. 4b and e, re-

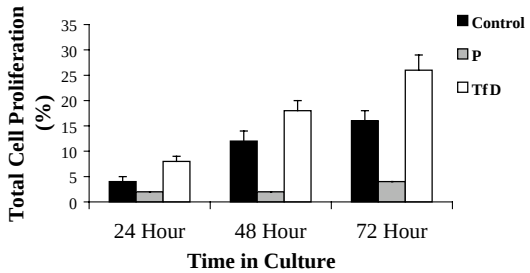

Fig. 3. Cell proliferation at 24, 48 and 72 h incubation as determined by BrdU incorporation of control cells, and cells incubated with either P or TfD nanoparticles.

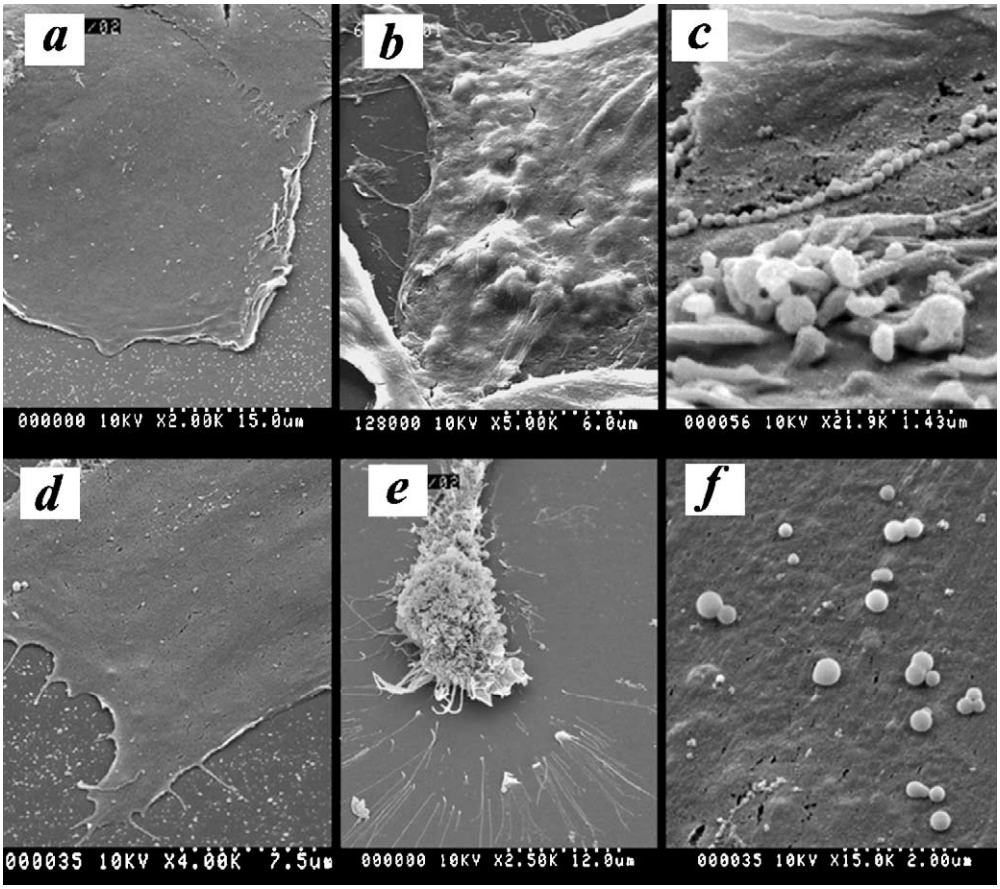

Fig. 4. Scanning electron microscope images of (a, d) control cells, (b, e) cells incubated with P nanoparticles and (c, f) cells incubated with TfD nanoparticles at 24 and 48 h, respectively. Note the TfD particles on the cell surface.

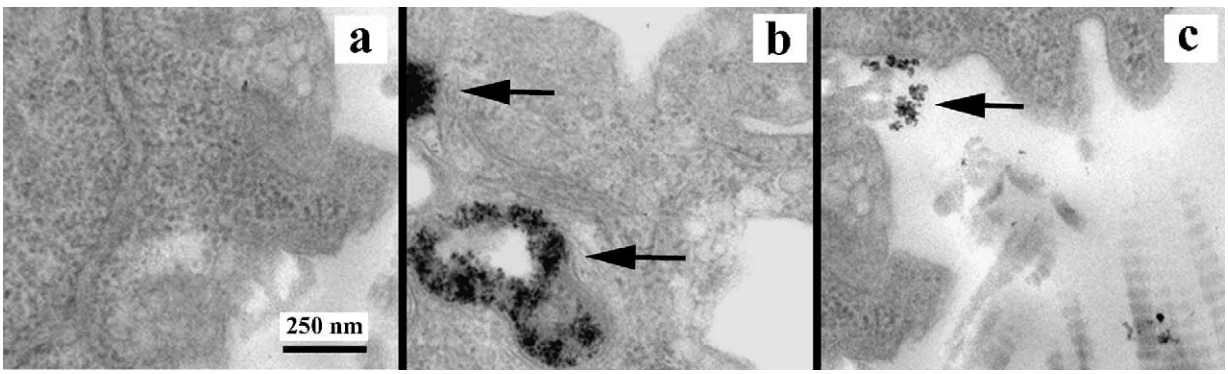

Fig. 5. Transmission electron microscope images of (a) control cells, (b) cells incubated with P nanoparticles and (c) cells incubated with TfD nanoparticles after 5 days in in collagen gel culture. Arrows denote areas of nanoparticle localisation.

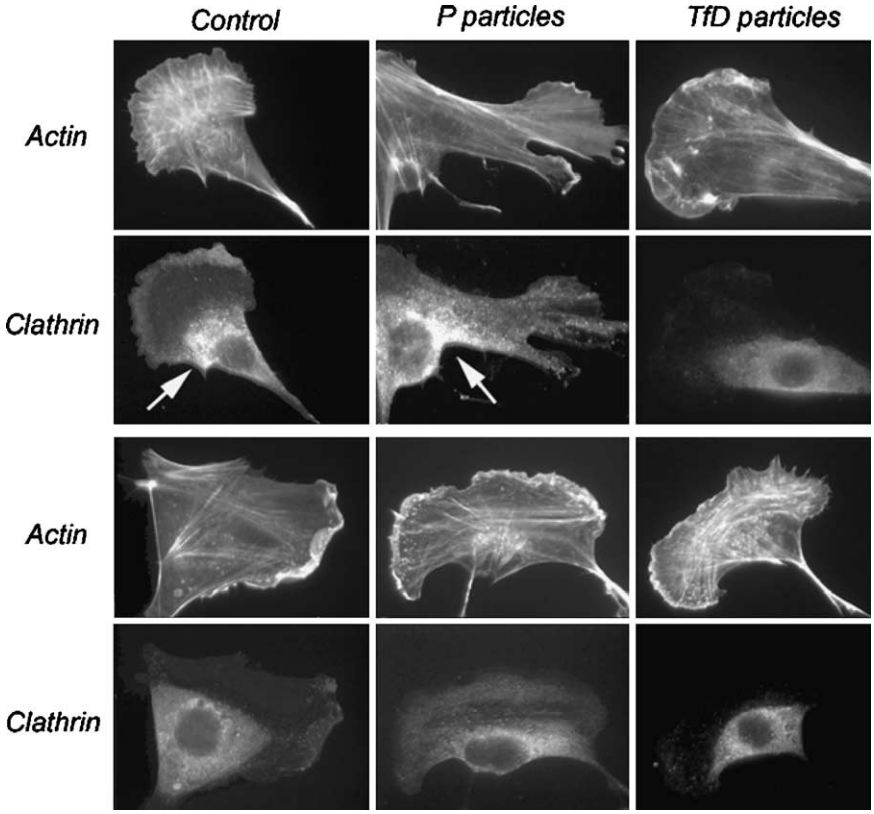

Fig. 6. Fluorescence images of F-actin/clathrin taken after 30 min incubation at either 37 °C (top panel) or 4 °C (lower panel) with the particles. Note the high clathrin levels indicated with the control and P particles at 37 °C, absent from cells incubated at 4 °C.

spectively). Interestingly, the TfD particles exhibited similar morphology to control cells and appeared to localise to the outer cell membrane in many cells observed at both time points (Fig. 4c and f). The TEM observations supported these observations at a later time point of 5 days in culture, with large vacuoles containing nanoparticles evident in response to the P nanoparticles, whilst the TfD particles appeared to localise to the cell exterior (Fig. 5).

With regards to clathrin levels, after 30 min incubation at 37 °C, the P particles clearly showed high levels of clathrin compared to the TfD particles (Fig. 6). This was not observed when the cells were incubated with particles at 4 °C, when all cells demonstrated low levels of clathrin. This would suggest that the fibroblasts are uptaking the P particles via an endocytotic mechanism (Vives et al., 1997; Teng and Wilkinson, 2003).

Tubulin, a cytoskeletal protein intimately associated with the movement of vesicles through the cell body, was disrupted at the cell lamella in response to the P particles at 37 °C, but not at 4 °C, (Fig. 7) again suggesting that uptake via endocytosis is occurring. Cells incubated with the TfD particles appeared similar to control cells in both temperature situations.

Fig. 8a–c demonstrates examples of fibroblasts incubated in the fluorescently coated nanoparticles after 30 min culture. The P fluorescent particles appear to be in clusters in the cell cytoplasm, possibly located in endocytotic vesicles, whereas the TfD images are similar to the control images, suggesting that little or no particle uptake is occurring. The level of fluorescence intensity due to particle uptake, measured via imageJ and expressed graphically in Fig. 8d, echoes this, indicating that there were high levels of P particle uptake, with very little evidence of TfD particle uptake.

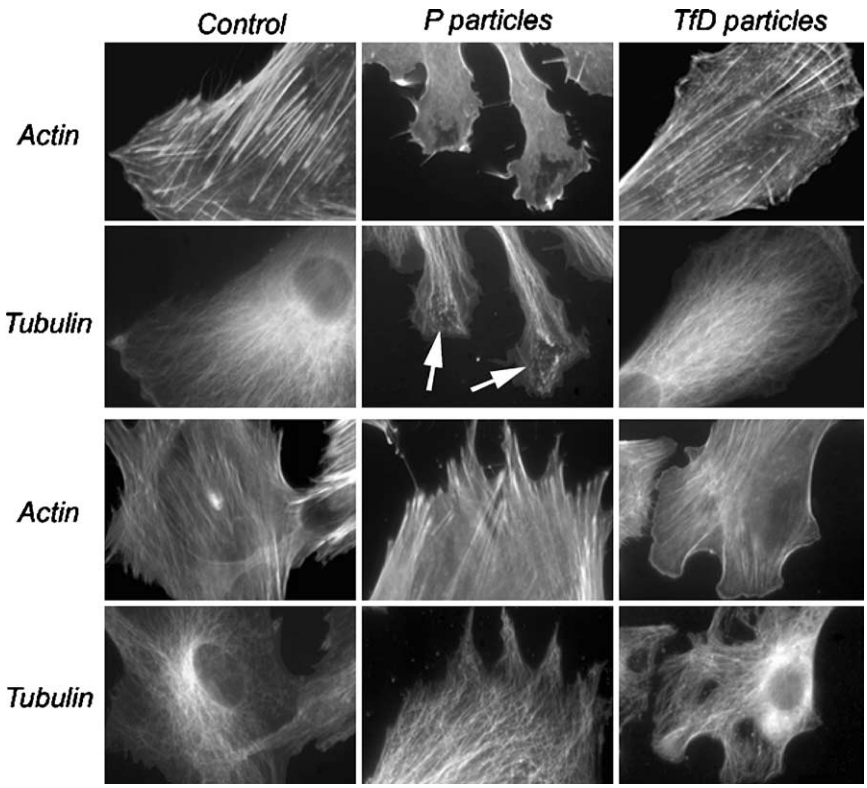

Fig. 7. Fluorescence images of F-actin/tubulin taken after 30 min incubation at either 37 °C (top panel) or 4 °C (lower panel) with the particles. Note the disrupted tubulin indicated with the P particles at 37 °C, absent from cells incubated at 4 °C.

Gene changes in response to the P particles were almost all down-regulation responses of a wide variety of genes (Table 1). There were several decreases observed with genes involved in cell replication, reflecting the decrease in BrdU cell proliferation results. There were only a couple of genes notably decreased ECM production, those being the protein fibrillin and also matrix metalloproteinase 7 (MMP-7), a member of the stromelysin subclass of MMPs. The majority of down-regulations were noted to be involved in cell signalling, such as various ion channels and growth factor binding proteins. Interestingly, the two up-regulations noted were beta-coat protein, a component of a cytosolic protein complex that reversibly associates with Golgi membranes to form vesicles, and also urokinase plasminogen activator cell receptor, which is commonly expressed in phagocytes and functions to focus fibrinolytic activity at the cell surface.

Conversely, most gene changes recorded in response to the TfD particles showed widespread gene activation, all of which were increases in activity (Table 2). The BrdU proliferation results were corroborated as an increase in many transcription factors and related genes was noted, thereby suggesting an increase in cell proliferation in response to the TfD nanoparticles.

Many cytoskeletal proteins were up-regulated, particularly those with relation to actin, which was reflected in the 24 h immunofluorescence results. In addition, the expressions of many genes involved in cell signalling were increased, including integrin subunits, tyrosine kinases and several members of the protein kinase C family ($\alpha/\delta/\theta/\zeta$), symptomatic of extracellular message signalling from the cell membrane to the nucleus. Furthermore, growth hormones, receptors and ion channels were up-regulated, alongside many Ras related proteins; all genes related to cell movement and interaction.

There were also significant increases in procollagen, collagen 1 and collagen 2 precursor gene expression observed, alongside other ECM proteins (laminin,

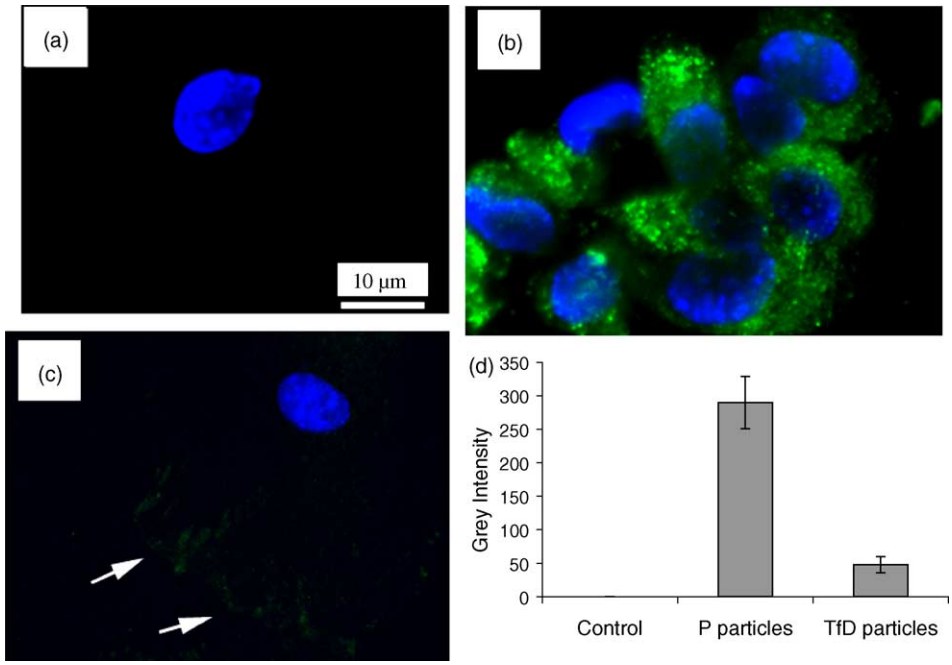

Fig. 8. Fluorescent images indicating particle uptake of (a) control cells, (b) fluorescently labeled P particles, (c) fluorescently labeled TfD particles after 30 min incubation (DAPI stained cell nuclei outlined), and (d) measurements of stain intensities using ImageJ, mean ± S.D.

elastin), showing an increase in matrix production in response to the particles. What is more, several matrix metalloproteinases (MMP-11, MMP-13) and their respective tissue inhibitors (TIMP 3) were also observed to change, suggesting that the fibroblasts are reorganising their matrix material.

Finally, with reference to Fig. 9, there was a significant increase in the intensity of CD71 immunostaining for the cells incubated with the TfD particles for 6 h as compared to the control cells.

4. Discussion

New functions arising from nanoparticle synthesis such as targetability and adhesion to tissues could introduce novel drug delivery systems. The combination use of magnetic nanoparticles derivatised with biological ligands, for example proteins commonly involved in opsonisation, could even further benefit such systems (Luck et al., 1998). In this study, the use of supraparamagnetic iron oxide particles derivatised with human transferrin provided results indicating better clinical potential than for underivatised particles.

Initial coomassie morphology staining indicated the appearance of vacuoles throughout the cell in response to the P particles. This is most likely due to massive particle internalisation (De Groot et al., 2001). Both SEM and TEM cell images support this suggestion, with aberrations apparent on the cell membrane, indicative of some form of internalisation, and vacuoles loaded with magnetite evident, respectively (McCarthy et al., 1986). The method of uptake is believed to be via endocytosis based on several lines of evidence. Blocking endocytosis by lowering the culture temperature to 4 °C is a common method of identifying the mechanism of particle uptake into cells (Vives et al., 1997; Teng and Wilkinson, 2003). Clathrin, a protein involved in the formation of coated pits during the early stages of endocytosis, was increased in cells incubated with P particles for 30 min at 37 °C, but decreased when the cells were incubated at 4 °C (Gagesu et al., 2000; McNiven et al., 2000). Similarly, tubulin, a cytoskeletal protein involved in vesicle movement, was disrupted at 37 °C, but organised at 4 °C (May and Machesky, 2001; Qualmann et

Table 1
Details of gene changes in response to incubation with P nanoparticles (all changes listed ≥ 50%) after 48 h culture

Gene	%
Exracellular matrix	
Fibrillin	−114
Matrix metalloproteinase-7 (matrilysin)	−134
Replication	
Basic transcription factor 3	−313
C-crk proto-oncogene (p38)	−190
c-fes proto-oncogene	−255
G-rich sequence factor-1 (GRSF-1)	−115
Putative ATP-dependent RNA helicase	−370
Zinc finger protein 7	−134
Zinc finger protein 76	−182
Cell signalling	
Beta-coat protein	+364
Chloride intracellular channel	−250
Chloride conductance inducer protein MAT-8	−200
Cytochrome p450	−116
Epidermal growth factor receptor	−202
ER Golgi intermediate protein	−324
Folate receptor	−232
Insulinlike growth factor binding protein	−169
PKC θ	−147
Sodium and chloride dependent GABA transporter-1	−367
Tyrosine protein kinase	−255
Urokinase plasminogen activator surface receptor	+110
Voltage gated potassium channel	−172

Most gene changes recorded were down-regulations.

al., 2000; Lamaze et al., 1997). Thus the P particles are being internalised via an endocytotic mechanism, whereas the TfD particles are not. Fluoresent particle uptake results substantiated the above, with measurements of P particle uptake, but no evidence of TfD particles being internalised.

The above results, in collaboration with an inhibition of cell proliferation and microarray data, suggest that the cells are rapidly endocytosing the P particles, resulting in a decrease in cell function. Such a finding is novel in that although previous studies have quantified levels of particle uptake, no such adverse effects have been observed, particularly at longer culture time points.

Conversely, with regards the TfD particles, with an increase in cell proliferation evident. The microarray data further supported this finding illustrating increases in a range of transcription factors and related genes. This would not be unexpected, however, as cell culture data have demonstrated that transferrin, a major iron transport protein, is a necessary requirement for cellular proliferation (Thomson et al., 1999; Seligman et al., 1992). However, the results presented here do show that derivatisation of the protein with the iron oxide nanoparticles does not alter the protein's beneficial influence on cells.

The F-actin appeared organised in response to the TfD particles, with well-defined stress fibres, but there were clear areas of actin spotting, indicative of actin polymerisation in response to the TfD particles. This was again substantiated with the microarray results, where increases in various actin associated proteins were noted, including gelsolin, profilin 1 and tropomodulin, all involved in actin capping and dynamics, signifying that the cells are active and motile (Cooper and Schafer, 2000; Stossel et al., 1999).

The most interesting result, however, was that the TfD particles appeared to attach to the cell membrane. This was evident after 24 h culture in the SEM images, and also after 5 days culture with the TEM images. This was apparent in most of the cells observed, on several individual occasions, and thus not an artefact of culturing or processing. It is known that cells express transferrin receptors (CD71) on their surface and when these receptors encounter a molecule of transferrin they bind it tightly. However, the complex is usually then engulfed via endocytois (Fuchs and Gessner, 2002), a process so efficient, that researchers have previously exploited the mechanism for the transfer of material into a cell (Moore et al., 2001; Truong-Lee et al., 1999). Therefore, the most likely suggestion of this localiastion observed would be that the cells are attaching to the cell expressed transferrin receptors (Testa et al., 1993). However, subsequent endocytosis of the transferrin/receptor complex does appear to follow, as the clathrin immunolocalisation, a protein intimately involved in endocytosis, of the cells exposed to TfD particles was similar to the control cells, suggesting that any ongoing endocytosis be due to normal cell metabolism only.

In order to investigate this further, immunostaining for CD71 was carried out (as CD71 was not included in the microarrays). It was clearly shown that there were elevated levels of the receptor after 6 h for cells incubated with the TfD particles as compared to the control cells. This would suggest that

Table 2
Details of gene changes in response to incubation with TfD nanoparticles (all changes listed ≥ 50%) after 48 h culture

Gene	%	Gene	%
Cytoskeleton		Cell signalling	
Actin aortic smooth muscle (alpha-actin 2)	56	Adenylyl cyclase-associated protein 1/2 (CAP 1/2)	70/62
Alpha actinin 2 (F-actin crosslinking protein)	71	Annexin VII	59
Alpha centractin	55	BDNF/NT-3 growth factor recepto62r precursor	
F-actin capping protein alpha-2 subunit	74	Calmodulin	58
Fibrillin 1 precursor	55	CAMP dependant protein kinase (type I beta)	53
Gelsolin precursor (actin polymerising factor)	64	CD 10/27L/40L/42C/44/106 receptor precursor	51/73/65/56/58/54
Keratin, type II cytoskeletal 7, 8 and 15	60/54/85	Clathrin coat assembly protein	53
Profilin I (G-actin binder; promoter of actin dynamics)	77	Chloride channel protein 4	57
Tropomodulin (actin capping protein)	54	Cytochrome C	57
Tropomyosin (fibroblast, non-muscle)	58	ECM protein 1 precursor	58
Villin	60	EGF receptor substrate substrate 15	52
Exracellular matrix		Extracellular signal-related kinase 1	60
Collagen alpha 1(XV) chain precursor	168	FGF receptor 3 precursor	62
Collagen alpha 1(XVIII) chain	54	Focal adhesion kinase	77
Collagen alpha 2 (XI) chain precursor	77	Growth hormone receptor precursor	56
Collagenase 3 Precursor (MMP-13)	52	Heparin binding growth factor 1 precursor	65
Laminin alpha 3/4 chain precursor	65/50	Insulin receptor precursor	68
Procollagen-lysine	52	Integrin β5 subunit precursor	53
Stromelysin-3 Precursor (MMP-11)	54	Interleukin-1 receptor antagonist protein precursor	64
Tropoelastin (elastin precursor)	51	MAP kinase 6	70
TIMP 3	72	Mast/stem cell growth factor receptor precursor	60
Replication		N-cadherin precursor	77
ADP-ribosylation factor 1	56	NT3 growth factor receptor precursor	68
Apoptosis regulator Bcl-w	56	Probable G protein coupled receptor GPR1/GPR13	65/70
Cell division protein kinase	58	Protein kinase C α/δ/θ/ζ	61/60/75/70
c-myc/c-myc binding protein	57/70	Protein kinase CLK2	52
Defender against cell death 1 (DAD-1)	56	Protein tyrosine phosphatase	63
DNA directed RNA polymerase II	54	Ras related protein rab -1B/-1C/-9/-11A/-11B/-27A	76/57/74/52/51/53
DNA polymerase α	53	Regulator of G protein signalling 3	57
DNA replicating licensing factor MCM5	63	Stem cell protein	61
Inhibitor of apoptosis protein	62	TGF beta 2/4 precursor	70/64
Mitochondrial transcription factor 1 precursor	54	Tryosine protein kinase	59
Possible global transcription factor SNF2l2	54	Vascular endothelial growth factor receptor 2 precursor	74
Proliferating-cell nucleolar antigen P120	59		
Stress activated protein kinase JNK2	63		
Transcription initiation factor IIB/IID/IIE	51/64/68		
Transcription factor AP-1	72		
Transcription factor BTF3	51		
Transcriptional repressor CTCF	63		
Transcription factor E2F1	57		
Transcription factor SP3	57		
Zinc finger protein 7/33A/133/151/OZF	51/56/65/69/52		

All gene changes recorded were up-regulations.

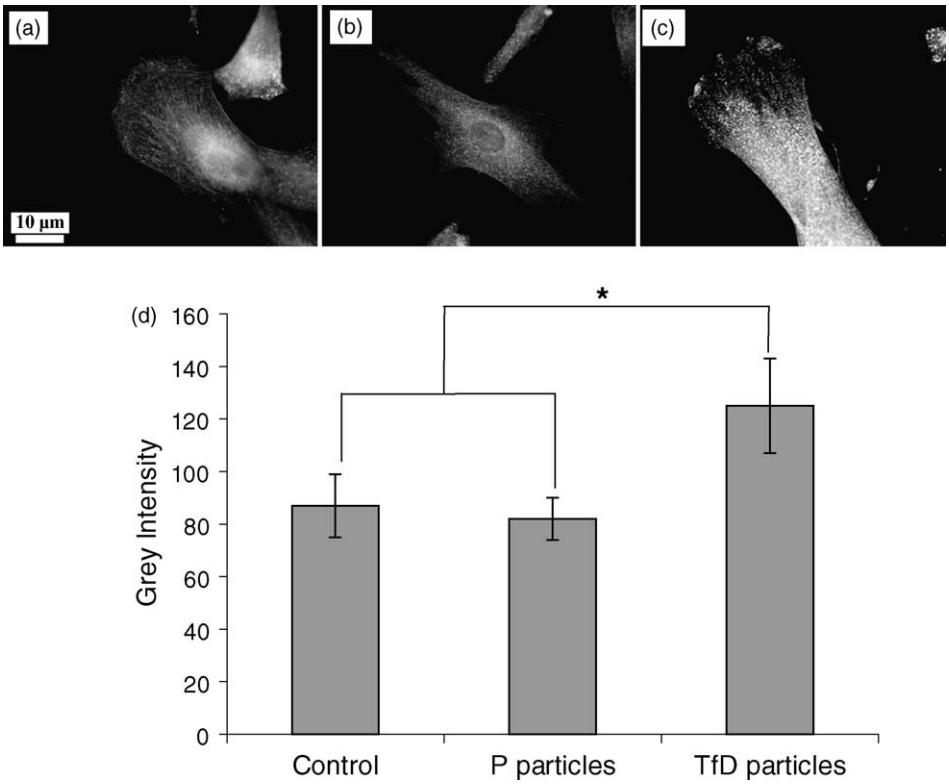

Fig. 9. Fluorescence images of CD71 stained control cells (a) and cells incubated with TfD for 6 h, and measurements of CDD71 stain intensities, mean ± S.D., $^{*}P \leq 0.05$ (c).

the TfD particles are attaching to the cell surface transferrin receptors, but in the absence of endocytosis allowing receptor/ligand recycling, the receptor may be increasing in expression to compensate for the demand.

The reason as to why the transferrin in this study does not appear to be internalised is unknown. It may be that, although the biological effects and chemistry of the protein are retained, the resultant size or shape due to derivatisation with the nanoparticles presents a stoichiometric hurdle for the receptor. Perhaps for receptor mediated endocytosis to occur, a conformational change would be required. Future studies on the physical TfD particle properties, alongside closer inspection of the localisation and quantification of the transferrin receptor (CD71) and its ligand, and possible recycling, on the cell membranes may help elucidate this targeting mechanisms further. In addition,

5. Conclusion

The results from a combination of morphological, immunological and genetic methods demonstrated that the synthesised supraparamagnetic iron oxide nanoparticles derivatised with transferrin encouraged an enhanced cell response as compared to underivatised particles. The positive influences made available by the presence of transferrin included increases in proliferation, cytoskeletal organisation, cell signalling and production of extracellular matrix.

A further result to be highlighted was the lack of internalisation of the TfD derivatised particles, despite attachment to the cell membrane. This type of cell response, when understood completely could be further exploited as a means to develop a promising drug delivery system, in addition to other biomedical applications such as MRI and tissue engineering. Such a system would not only target cells, but also convey ben-

efits including proliferation, signalling and ECM production, thus leading to a better overall performance of the drug.

Acknowledgements

The financial support of the European Commission Fifth Framework Growth Programme, grant number GRD5-CT2000-00375 and also the assistance of Mr. Eoin Robertson (EM Unit) and MBSU Unit is greatly appreciated.

References

Babes, L., Denizot, B., Tanguy, G., Le Jeune, J.J., Jallet, P., 1999. Synthesis of iron oxide nanoparticles used as MRI contrast agents: a parametric study. J. Coll. Int. Sci. 212, 474–482.

Bell, E., Ivarsson, B., Merrill, C., 1979. Production of a tissue-like structure by contraction of collagen lattices by human fibroblasts of different proliferative potential in vitro. Proc. Natl. Acad. Sci. U.S.A. 76, 1274.

Bonnemain, B., 1998. Superparamagnetic agents in magnetic resonance imaging: physiochemical characteristics and clinical applications—a review. J. Drug Target. 6, 167–174.

Bulte, J.M.W., Zhange, S.C., van Gelderen, P., Herynek, E.K., Duncan, I.D., Frank, J.A., 1999. Neurotransplantation of magnetically labeled oligodendrocyte progenitors: magnetic resonance tracking of cell migration and myelination. Proc. Natl. Acad. Sci. U.S.A. 96, 15256–15261.

Chouly, C., Pouliquen, D., Lucet, I., Jeune, J.J., Jallet, P., 1996. Development of superparamagnetic nanoparticles for MRI: effect of particle size, charge and surface nature on biodistribution. J. Microencapsul. 13, 245–255.

Cooper, J.A., Schafer, D., 2000. Control of actin assembly and disassembly at filament ends. Curr. Opin. Cell Biol. 12, 97–103.

Curtis, A.S.G., Wilkinson, C., 2001. Nanotechniques and approaches in biotechnology. Trends Biotech. 19, 97–101.

Davis, S.S., 1997. Biomedical applications of nanotechnology—implications for drug targeting and gene therapy. Trends Biotechnol. 15, 217–224.

De Groot, C.J., Van Luyn, M.J.A., Van Dijk-Wolthuis, W.N.E., Cadee, J.A., Plantinga, J.A., Otter, W.D., Hennink, W.E., 2001. In vitro biocompatibility of biodegradable dextran-based hydrogel tested with human fibroblasts. Biomaterials 22, 1197–1203.

Eisen, M.B., Spellman, P.T., Brown, P.O., Botsetin, D., 1998. Cluster analysis and display of genome-wide expression patterns. Proc. Natl. Acad. Sci. U.S.A. 95, 863–868.

Fuchs, H., Gessner, R., 2002. Iodination significantly influences the binding of human transerrin to the transferrin receptor. Biochim. Biophys. Acta 1570, 19–26.

Fulimoto, L.M., Roth, R., Heuser, J.E., Schmid, S.L., 2000. Actin assembly plays a variable, but not obligatory role in receptor-mediated endocytosis in mammalian cells. Traffic 1, 161–171.

Gagesu, R., Gruenberg, J., Smyte, E., 2000. Membrane dynamics in endocytosis: structure–function relationship. Traffic 1, 84–88.

Grinnell, F., Lamke, C.R., 1984. Reorganisation of hydrated collagen lattices by human skin fibroblasts. J. Cell Sci. 66, 51–63.

Lacava, L.M., Lacava, Z.G.M., Da Silva, M.F., Silva, O., Chaves, S.B., Azevedo, R.B., Pelegrini, F., Gansau, C., Buske, N., Salbolovic, D., Morais, P.C., 2001. Magnetic resonance of a dextran-coated magnetic intravenously administered in mice. Biophys. J. 80, 2483–2486.

Lamaze, C., Fujimoto, L.M., Yin, H.L., Schmid, S.L., 1997. The actin cytoskeleton is required for receptor-mediated endocytosis in mammalian cells. J. Biol. Chem. 272, 20332–20335.

Li, H., Qian, Z.M., 2002. Transferrin/transferrin receptor-mediated drug delivery. Med. Res. Rev. 22, 225–250.

Lubbe, A.S., Bergemann, C., Brook, J., McClure, D.G., 1999. Physiological aspects in magnetic drug targeting. J. Magn. Magn. Mater. 194, 149.

Lubbe, A.S., Alexiou, C., Bergemann, C., 2001. Clinical applications of magnetic drug targeting. J. Surg. Res. 95, 200–206.

Luck, M., Paulke, B.R., Schroder, W., Blunk, T., Muller, R.H., 1998. Analysis of plasma protein adsorbtion on polymeric nanoparticles with different surface characteristics. J. Biomed. Mater. Res. 39, 478–485.

May, R.C., Machesky, L.M., 2001. Phagosytosis and the actin cytoskeleton. J. Cell Sci. 114, 1061–1077.

McCarthy, D.A., Holburn, C.M., Pell, B.K., Moore, S.R., Kirk, A.P., Perry, J.D., 1986. Scanning electron microscopy of rheumatoid arthritis peripheral blood polymorphonuclear leucocytes. Ann. Rheum. Dis. 45, 899–910.

Michell, B.B., Shiigi, S.M., 1980. Selected methods in cellular immunology. WH Freeman and Company, San Francisco.

McNiven, M.A., Cao, H., Pitts, K.R., Yoon, Y., 2000. The dynamin family of mechanoenzymes: pinching in new places. TIBS 25, 115–120.

Moghimi, S.M., Hunter, A.C.H., Murray, J.C., 2001. Long-circulating and target-specific nanoparticles: theory to practice. Pharm. Rev. 53, 283–318.

Moore, A., Josephson, L., Bhorade, R.M., Basilion, J.P., Weissleder, R., 2001. Human transferrin receptor gene as a marker gene for MR Imaging. Radiology 221, 244–250.

Morrissette, N.S., Gold, E.S., Aderem, A., 1999. The macrophage—a cell for all seasons. Trends Cell Biol. 9, 199–201.

Muller, R.H., Jacobs, C., Kayser, O., 2001. Nanosuspensions as particulate drug formulations in therapy. Rationale for development and what we can expect for the future. Ad. Drug Del. Rev. 47, 3–19.

Nakagawa, T., Pawelek, P., Grinnell, F., 1989. Long-term culture of fibroblasts in contracted collagen gels: effects on cell growth and biosynthetic activity. J. Invest. Dermat. 792–798.

Qualmann, B., Kessels, M.M., Kelly, R.B., 2000. Moleculal links between endocytosis and the actin cytoskeleton. J. Cell Biol. 150, F111–F116.

Reimers, G.W., Khalafalla, S.E., 1972. Preparing magnetic fluids by a peptizing method. US Bureau of MinesTech. Rep. 59.

Seligman, P.A., Kovar, J., Gelfand, E.W., 1992. Lymphocyte proliferation is controlled by both iron availability and regulation or iron uptake pathways. Pathobiology 60, 19–26.

Stossel, T.P., Hartwig, J.H., Janmey, P.A., Kwiatkowski, D.J., 1999. Cell crawling two decades after Abercrombie. Biochem. Soc. Symp. 65, 267–280.

Teng, H., Wilkinson, R.S., 2003. Delayed endocytosis is regulated by extracellular Ca^{2+} in snake motor boutons. J. Physiol. 551, 103–114.

Testa, U., Pelosi, E., Peschle, C., 1993. The transferrin receptor. Crit. Rev. Oncog. 4, 241–276.

Thomson, A.M., Rogers, J.T., Leedman, P.J., 1999. Iron-regulatory proteins, iron-responseive elements and ferritin mRNA translocation. Int. J. Biochem. Cell Biol. 31, 1139–1152.

Torchilin, V.P., 2000. Drug targeting. E. J. Pharm. Sci. 11, S81–S91.

Truong-Lee, V.L., Walsh, S.M., Schweibert, E., Mao, H.-Q., Guggino, W.B., August, J.T., Leong, K.M., 1999. Gene transfer by DNA-gelatin nanospheres. Arc. Biochem. Biophys. 361, 47–56.

Vives, E., Brodin, P., Lebleu, B., 1997. A truncated HIV-1 Tat protein basic domain rapidly translocates through the plasma membrane and accumulates in the cell nucleus. J. Biol. Chem. 272, 16010–16017.

Wang, Y.X., Hussain, S.M., Krestin, G.P., 2001. Superparamagnetic iron oxide contrast agents: physicochemical characteristics and applications in MR imaging. Eur. Radiol. 11, 2319–2331.